N.-P. Finger[1,2], M. K. Kaban[1,3], M. Tesauro[4,5], W. D. Mooney[6], M. Thomas[1,2]

[1]German Research Centre for Geosciences, Potsdam, Germany.

[2]FU Berlin, Berlin, Germany.

[3]Schmidt Institute of Physics of the Earth, RAS, Moscow, Russia.

[4]University of Trieste, Trieste, Italy.

[5]University of Utrecht, Utrecht, Netherlands.

[6]US Geological Survey, Menlo Park, USA.

Corresponding author: Nils-Peter Finger (finger@gfz-potsdam.de)

Key Points:

- A new Moho map was constructed from available seismic data to improve thermo-compositional modeling of the African cratonic lithosphere
- Lithosphere of the West African, central to northern Congo, and Zimbabwe cratons is cold, up to 250 km thick, and chemically depleted
- Hot, thin (<200 km) and mostly undepleted lithosphere of Uganda, Tanzania, southern Congo and Kaapvaal cratons indicates refertilization

Abstract

Recently, the continually increasing availability of seismic data has allowed high-resolution imaging of lithospheric structure beneath the African cratons. In this study, S-wave seismic tomography are combined with high resolution satellite gravity data in an integrated approach to investigate the structure of the cratonic lithosphere of Africa. A new model for the Moho depth and data on the crustal density structure are employed along with global dynamic models to calculate residual topography and mantle gravity residuals. Corrections for thermal effects of an initially juvenile mantle are estimated based on S-wave tomography and mineral physics. Joint inversion of the residuals yields necessary compositional adjustments that allow to recalculate the thermal effects. After several iterations, we obtain a consistent model of upper mantle temperature, thermal and compositional density variations, and Mg# as a measure of depletion, as well as an improved crustal density model. Our results show that thick and cold depleted lithosphere underlies West African, northern to central eastern Congo, and Zimbabwe Cratons. However, for most of these regions, the areal extent of their depleted lithosphere differs from the respective exposed Archean shields. Meanwhile, the lithosphere of Uganda, Tanzania, most of eastern and southern Congo, and the Kaapvaal Craton is thinner, warmer, and shows little or no depletion. Furthermore, the results allow to infer that the lithosphere of the exposed Archean shields of Congo and West African cratons was depleted before the single blocks were merged into their respective cratons.

Plain Language Summary

Cratons are the ancient cores of continents that, with few exceptions, are underlain by a cold, strong lithospheric root with a thickness of about 250 km. The physical properties of lithospheric roots, principally temperature and composition, shed light on the origin and evolution of the most ancient portions of the Earth's lithosphere, the Precambrian cratons. We use an iterative method to process S-wave seismic tomography and satellite gravity data to calculate the thermal and compositional state of the lithosphere. Our results reveal great diversity in the thickness and physical properties of the African lithosphere. The West African, northern Congo and Zimbabwe cratons are underlain by relatively cold, thick and chemically depleted lithosphere. In contrast, the Uganda, Tanzania, southern Congo and Kaapvaal cratons are warmer, thinner and have a less depleted (or non-depleted) composition, indicating either re-fertilization (metasomatism) or formation in a non-depleted state. These results document the formation of the Africa continent during the past 3.7 Ga from a diverse collection of cratons, each with a unique evolutionary history.

1. Introduction

Cratons are the ancient continental cores, around which continents accrete and grow. They are stable for billions of years, and due to their geologic evolution often provide an abundancy of resources, e.g., rare earth elements and diamonds. Cratons are usually underlain by thick continental lithosphere, their so-called "roots", which can reach up to about 250 km into the Earth (e.g., Steinberger & Becker, 2018). With a few exceptions (Kaban et al., 2015), these roots resist mantle convection, and thus deviate mantle flow. Therefore, a better understanding of cratons, their evolution and dynamics may provide further insight to large scale dynamic and tectonic processes. Cratons appear to be buoyant with respect to the underlying mantle despite the fact that their long-term cooling causes an increase in density. A commonly cited explanation is the iso-pycnic hypothesis (Jordan, 1978) that is based on the counter-balancing effect of chemical buoyancy. The density increase caused by reduced temperatures is balanced by density decrease from depletion in heavy constituents, mostly iron (Fe; Griffin et al., 2003). Depletion is commonly measured by means of Mg#, the percentage of Magnesium (Mg) in the total amount of Mg and Fe (100*Mg/(Mg+Fe)) in mantle minerals. Mg#s around 89 are common for fertile mantle rocks, while strongly depleted samples exhibit values around 94 (Griffin, O'Reilly, Abe, et al., 2003; McDonough & Sun, 1995). Still, despite being a long-time focus of geoscientific studies, in a global perspective, various cratons have been studied to very different extents and several aspects concerning their physical properties are still under debate (e.g., Celli et al., 2020; Mooney & Vidale, 2003). On the African continent, a large body of geologic, geochemical and geophysical data and numerous publications exist for the Kaapvaal and adjacent Zimbabwe cratons, along with a large array of seismic stations (Globig et al.,

2016). Yet, lithospheric thickness of these cratons is still a matter of debate (White-Gaynor et al., 2021). Meanwhile, much fewer seismic stations and other data are available for the significantly larger Congo and West African cratons.

However, employing seismic tomography and satellite gravity data allows an assessment of the thermal and compositional state of the cratonic lithosphere, even for very remote oder not accessible areas like Antarctica (e.g., Haeger et al., 2019). On the one hand, seismic velocities provide a solid and widely used basis for temperature estimates of the lithosphere (Cammarano et al., 2003; Steinberger & Becker, 2018) since they are governed by thermal variations (Goes et al., 2000). In comparison, compositional variations have a rather minor influence on seismic velocities (e.g., Schutt & Lesher, 2010). Both thermal and compositional variations cause density variations, which can be detected, but not separated by gravity measurements. Thus, integrated modeling of gravity and seismic data profits from their respective advantages while reducing the disadvantages. A respective approach (Kaban et al., 2014; Tesauro et al., 2014a) was recently used to assess the thermal and compositional state of cratonic lithosphere of several continents, e.g., South America (Finger, Kaban, Tesauro, Haeger, et al., 2021), Antarctica (Haeger et al., 2019), and Australia (Tesauro et al., 2020). The method yields self-consistent thermal and compositional results for the mantle lithosphere from the Moho down to about 325 km. Despite providing sophisticated indications for the current state and depth extent of cratonic lithosphere, the results can also be a basis for further studies. For example, results for Antarctica (Haeger et al., 2019) were used to calculate decompositional gravity anomalies in an attempt to determine thickness of sediments beneath the ice (Haeger & Kaban, 2019).

As mentioned above, the African continent comprises several cratons (Figure 1) whose lithospheric thickness, physical state, and evolution are still a matter of debate (Boyce et al., 2021; Celli et al., 2020; Hu et al., 2018; Jessell et al., 2016; White-Gaynor et al., 2021). Here, we image the cratons of Africa, and produce a new, purely seismic model of depth to the Moho in the process, which enables calculation of residual topography and mantle gravity. These are assessed for thermal and compositional mantle density variations in an iterative joint inversion scheme. Moreover, the method yields an improved crustal density model and allows to assess to which extent depth to the Moho affects the results of the integrated mantle model.

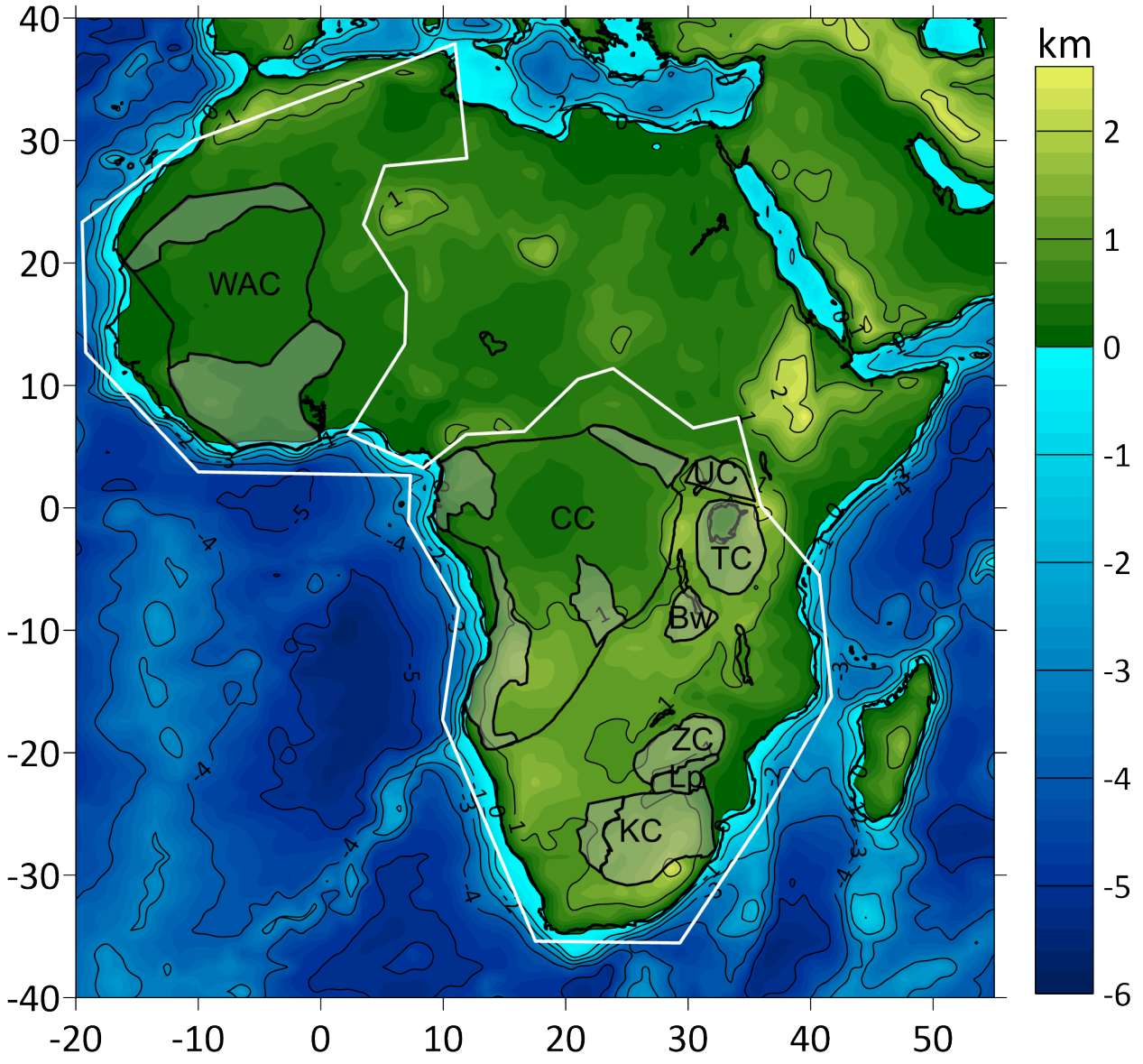

Figure 1: Topography and bathymetry of Africa and surrounding area. Numbers indicate elevation contours in km. This study is focused on the cratonic regions denoted by the white polygon. Mostly exposed cratons are indicated by black outlines, with Archean shields and microcontinents shaded grey (Begg et al., 2009). WAC:West African craton, CC: Congo craton, UC: Uganda craton, TC: Tanzania craton, Bw: Bangweulu block, ZC: Zimbabwe craton, Lp: Limpopo belt, KC: Kaapvaal craton.

1. Geology Overview

Begg et al. (2009) and references therein provide a detailed summary of the main terranes, belts and basins of the African continent. Here, a simplified overview based on their work is provided except where noted. The cratonic part of Africa, on which this study focuses, consists of the West African craton, the cratons from the central African Oubanguides belt southwards, and most of their surrounding Proterozoic fold belts (white polygon in Figure 1). The non-cratonic part is constituted by wide parts of the extensive "Saharan" domain, namely the West African mobile zone and the East Saharan metacraton, as well as the East African orogenic zone down to the eastern border of the Tanzania craton. While cratons are inferred to occupy a significant portion of the cratonic region, only some of their areas are actually exposed Archean shields, while most of their surface is covered by sedimentary basins. In case of the West African craton, the northern Reguibat and southern Man-Leo shields are separated by the Proterozoic Taoudeni basin covering the craton's central area. Recent S-wave tomography (Celli et al., 2020) indicates two separate roots. The Congo Craton in central Afrika hosts four Archean shield areas, parts of which are probably covered by the Congo basin: the Gabun-Cameroon in the Northwest, Bomu-Kibali in the Northeast, Kasai in the central East, and Angolan along the western border south of the Gabun-Cameroon. Begg et al. (2009) infer different ages and a unique evolution of the four shields. However, Congo craton lithosphere appeared as a single large block in tomographies (e.g., Fishwick, 2010; Schaeffer & Lebedev, 2013) until recent advances allowed to image separate root structures (Celli et al., 2020). To the East, an emerging plate boundary now separates the Congo craton from the 2.9 to 2.8 Ga old Uganda and Tanzania cratons, which have been accreted to it during 1.8 Ga paleo-Kibaran orogeny, together with the Bangweulu block, a Neoarchean microcontinent. Tomography (Celli et al., 2020) indicates that the Uganda and Tanzania cratons both lack a deep root. For the Tanzania craton, an east-to-west increase of lithosphere thickness (Boyce et al., 2021) and presence of about 30 Ma old kimberlites (Tappe et al., 2018) point to a geologically recent root loss due to plume impingement that also initiated the East African rift system (EARS). The Kaapvaal and Zimbabwe cratons collided 2.6 to 2.7 Ga, capturing the Limpopo microcontinent between them and currently form the South African craton. Several large igneous provinces (LIPs) were emplaced on top or in the vicinity of the cratons: the Bushveld (around 2.05 Ga) and Karoo (180 Ma, Giuliani et al., 2014) on the Kaapvaal craton, Etendeka (135 Ma, Morgan, 1983) on the Angolan shield of the Congo craton, along with formation of the EARS next to the Tanzania craton (30 Ma until today, Ebinger & Sleep, 1998), and the Central Atlantic magmatic province (CAMP, 200 Ma, Wilson, 1997) close to the West African craton. CAMP, Etendeka, and Karoo preceded or accompanied the separation from South America and Antarctica, ending the Pangean supercontinent. Emplacement of such LIPs is generally thought to be caused by mantle plumes (e.g., Ebinger & Sleep, 1998), which are among the few geologic processes able to significantly affect or even erode cratonic lithosphere

(Lee et al., 2011).

1. Methods

   (a) Mantle Model

The method employed here is the same as in our recent study of the South American cratonic regions (Finger, Kaban, Tesauro, Haeger, et al., 2021). A sketch of the integrated iterative approach is given in Figure 2. In a first preparation step, an initially juvenile fertile mantle with Mg# 89 and respective bulk composition of 58.5% Olivine, 11.5% Clinopyroxene, 15% Orthopyroxene, and 15% Garnet (Griffin, O'Reilly, Abe, et al., 2003) is assumed to estimate temperatures and thermal density variations in the upper mantle based on S-wave tomography AF2019 (Celli et al., 2020) and mineral physics (Cammarano et al., 2003; Hyndman et al., 2009; Stixrude & Lithgow-Bertelloni, 2005). This is done for six layers centered at 50 to 300 km depth with an interval of 50 km. In a second step, depth to the Moho is estimated using the approach of Stolk et al. (2013), utilizing topography (ETOPO1 Amante & Eakins, 2009), sediment thickness and density (Crust1.0, Laske et al., 2013), and seismic data (Globig et al., 2016; Mooney, 2015 with updates up to 2019). This allows to remove crustal effects from the gravity data (EIGEN6-C4, Förste et al., 2014) and furthermore calculate residual topography (Kaban & Mooney, 2001) as a measure of compensation of density anomalies by the uppermost mantle. In addition, the effects of lower mantle density anomalies (below 325 km) are removed from the two fields by means of global dynamic models (Kaban et al., 2015) based on tomography (S40RTS, Ritsema et al., 2011). Since these effects are only present in the very long wavelengths (Kaban, El Khrepy, et al., 2016), they do not notably affect the results. After these preparations, the iterative process begins with removing the afore calculated thermal variations from the residual mantle gravity and residual topography. The remaining anomalies are assumed to be mainly of compositional origin. Thus, a joint inversion enables determination of necessary compositional variations. Since gravity and residual topography react differently to mass changes (Kaban & Mooney, 2001), it is possible to at least partly overcome the ambiguity of simple gravity inversion. For said inversion, grids are transformed to spherical harmonics. Moreover, a seventh layer centered at 15 km is included in the inversion to cover density variations not included in the initial crustal model. Where mantle density variations proposed by the joint inversion are negative, Mg# and thus composition are adapted towards an end-member of strong iron depletion (Mg# 94), consisting of 69.5% Olivine, 4% Clinopyroxene, 21% Orthopyroxene and 5.5% Garnet (McDonough & Sun, 1995). The next iteration starts by adjusting the thermal model to the changes in composition. Convergence is reached when the maximum difference in Mg# of two subsequent compositional models is 0.1 at any given point. This is usually achieved after four iterations. The final mantle model yields six grids of 1° lateral resolution at depths of 50, 100, 150, 200, 250, and 300 km for each of temperature, thermal and compositional density variation, and Mg#. Each grid represents the center of a 50 km thick layer, except the topmost one, for

which the upper boundary and thus thickness is defined by the depth to the Moho. Resulting density variations for the additional layer centered at 15 km can be used to improve the crustal density model. For a more detailed description of the method, the interested reader is referred to Kaban et al. (2014) and Tesauro et al. (2014a). An assessment of the influence of damping is given in the supplemental material of Kaban et al. (2015).

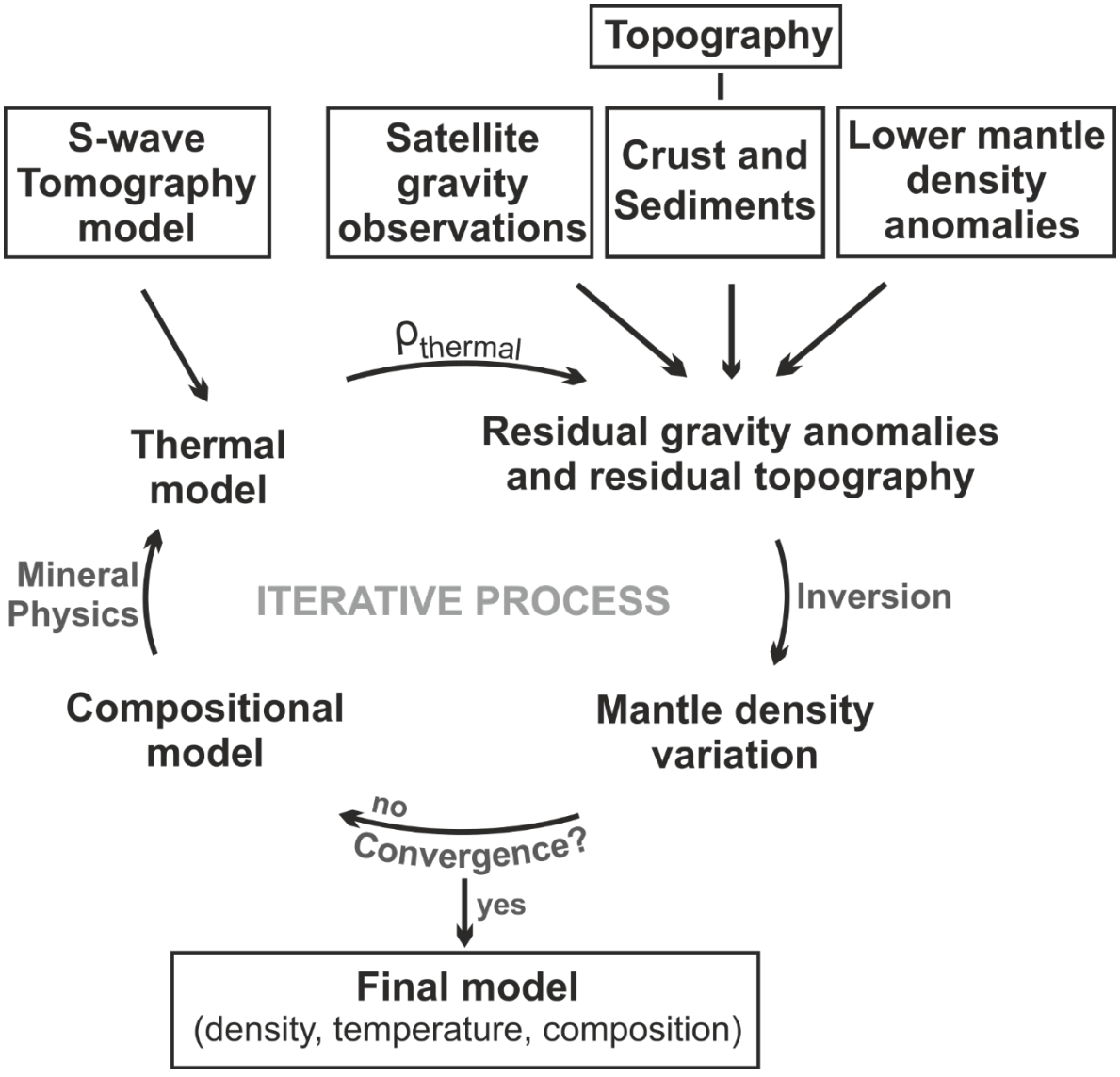

Figure 2: Sketch of the integrated iterative approach (modified from Haeger et al., 2019). To enable the iterative process, S-wave velocities are converted into a thermal model. In addition, calculation of depth to the Moho (Chapter 2.2)

allows to determine crustal effects, and thus residual mantle gravity and residual topography. Convergence is reached when the inversion does not indicate changes of Mg#>0.1.

1. Depth to the Moho

An accurate as possible estimate of depth to the Moho is critical in this iterative approach that yields the best-fitting upper mantle model. Various Moho depth models have been presented for Africa over the past decades, either in a regional (e.g., Globig et al., 2016; Pasyanos & Nyblade, 2006; Tugume et al., 2013) or global context (e.g., Laske et al., 2013; Pasyanos et al., 2014) and based on different data and modeling techniques. However, a purely seismic determination is desired for the approach applied here, but previous seismic models show large differences (van der Meijde et al., 2015). Therefore, we calculate a new model of depth to the Moho via the method of Stolk et al. (2013). It is based on the reasonable assumption that measurements of crustal thickness (including topography) or depth to the Moho (at sea-level) reflect isostatic topographic effects. Subtracting these from data reduces their variance and thus variance of the subsequent interpolation. Afterwards, effects can be restored to the interpolated field. This way, interpolated depth to the Moho follows main topographic features in areas of sparse data. Seismic measurements (Globig et al., 2016; Mooney, 2015 with updates up to 2019) are binned to 1°x1° cells to reduce the effects of outliers. Then, determination of isostatic effects starts with calculating adjusted topography which would be the residing topography if sediments and water were compacted to the density of the upper crust (2.67 g/cm^3). Due to a lack of relevant data, it was not possible to create a sediment density model like for South America (Finger et al., 2020; Finger et al., 2021). Instead, data for the sedimentary layers from Crust1.0 (Laske et al., 2013) are used. The type of isostacy assumed is not relevant, since the effects will be restored to the interpolated field (Kaban, Stolk, et al., 2016; Stolk et al., 2013), and local Airy Isostasy is assumed. After correcting the binned data, outliers are removed by hold-one-out cross-correlation. Depth to the Moho is interpolated by means of ordinary kriging as implemented in PyKrige (Murphy et al., 2020), treating the binned measurements as exact. Finally, the isostatic correction is restored to the interpolated field. Later, interpolation results in areas of scarce or no data can be assessed using the results of the iterative scheme (Kaban, El Khrepy, et al., 2016). Since the iterative approach requires global fields, results for depth to Moho were merged into a global map consisting of Crust1.0 with updates from previous studies for most continents (Finger, Kaban, Tesauro, Haeger, et al., 2021; Kaban, Stolk, et al., 2016; Tesauro et al., 2014b)

1. Correction for Crust and Deep Mantle Effects

After construction of the crustal model, we compute its effects and remove these from the observed topography and gravity field. The free air gravity disturbances, which are used as the initial field, are taken from EIGEN-6C4 (Förste et al., 2014). Although the model is based on a combination of satellite and ground/airborne determinations, for the resolution of this study (1°x1°) it

is determined only from satellite data. Using these data, the initial field has sufficient resolution for the whole study area.

We compute the effect of density deviations from a 1D reference model (Table 1) following the method used in previous studies (e.g., Finger et al., 2021; Kaban, Stolk, et al., 2016; Mooney & Kaban, 2010). Although choice of such a model only causes a constant shift of the computed fields, which is not considered here (Mooney & Kaban, 2010), using the same reference model provides a useful opportunity for comparison with results obtained in previous studies for different continents. The initial density of topography is 2.67 g/cm³. Later on, effects of low-density sediments have also been considered. The ocean water density is 1.03 g/cm³.

	Upper crustal layer	Lower crustal layer	Subcrustal layer
Depth (km)	0–15	15–40	40–75
Density (g/cm^3)	2.7	2.94	3.32

Table 1: 1D reference model of the crust and uppermost mantle.

The gravity effects of all crustal layers were estimated by a 3D approach on the sphere as described in previous studies (Finger, Kaban, Tesauro, Haeger, et al., 2021; Kaban et al., 2015; Kaban, Stolk, et al., 2016). Comparison with other independent methods has shown that its accuracy is within few mGal (Root et al., 2016), which is sufficient for the present study. Even remote structures, especially at large depths, can produce a significant gravity effect in the study area. Therefore, the calculations were made for a global model (e.g., Mooney & Kaban, 2010). Outside the study area, we employed Crust1.0 (Laske et al., 2013), which was improved by several continental models with higher resolution (e.g., Finger et al., 2021; Kaban, Stolk, et al., 2016; Mooney & Kaban, 2010). Since far-field effects depend only on large-scale structures, possible uncertainties of the global model don't affect the obtained results remarkably.

In addition to the residual mantle gravity field, the residual topography has been also estimated based on the same data on crustal structure. The residual topography is the part of topography that is not fully compensated by the crustal heterogeneity. For the crust, the residual topography has been computed by assuming local isostatic conditions (Kaban, Stolk, et al., 2016). For the mantle, the effect on topography has been computed in a dynamic environment by considering mantle viscosity as described in Kaban et al. (2016). As was mentioned above, the use of both fields principally improves vertical resolution of the inversion (Kaban, El Khrepy, et al., 2016).

1. Results
   (a) Depth to the Moho

Depth to the Moho (Figure 3) varies across the African continent and its patterns partially depend on the distribution of available seismic data. In southern Africa and along the EARS, measurement and/or station density are high and mostly result in depths to the Moho ranging from 35 to 42 km. For most of the Saharan areas, data are very scarce and results are mostly between 28 and 35 km. Similar differences are also found across cratons. While values in the southern West African craton are greater than 35 km, estimates in its northern part, where no data are available, range from 28 to 32 km. Comparably, depth to the Moho is estimated to lie between 26 and 33 km for the Uganda craton and northeastern to central-western data devoid area of the Congo craton. Meanwhile, interpolation results are above 35 km for the northwestern and southern Congo craton. The well-covered Tanzania, Zimbabwe, and Kaapvaal cratons mostly yield results from 35 to 42 km. A small minimum of 34 km is located in the southern Kaapvaal craton. Overall minimal values on the continent are <25 km in the northern EARS, supported by data, and towards the Horn of Africa, with no data. The latter are most probably an artifact from interpolation between thin oceanic crust in the East and >35 km thick crust at the EARS to the West.

As expected based on the high data density, interpolation uncertainties south of the equator are rather small, mostly ranging from 2.8 to 3.6 km, except for the central Congo craton. From here, a band of uncertainties from 4 to some 5 km stretches roughly east and north towards the Horn of Africa, containing the mostly data devoid areas in central Africa. North of the equator, low uncertainties <3 km are present in the well-covered northwestern Congo craton, central Sahara and west of the West African craton. Uncertainties in the West African craton itself are around 4 km, with maxima of more than 5 km in its South and Northeast. Highest values are >6 km and located at the Horn of Africa and the central part of the Mediterranean coast.

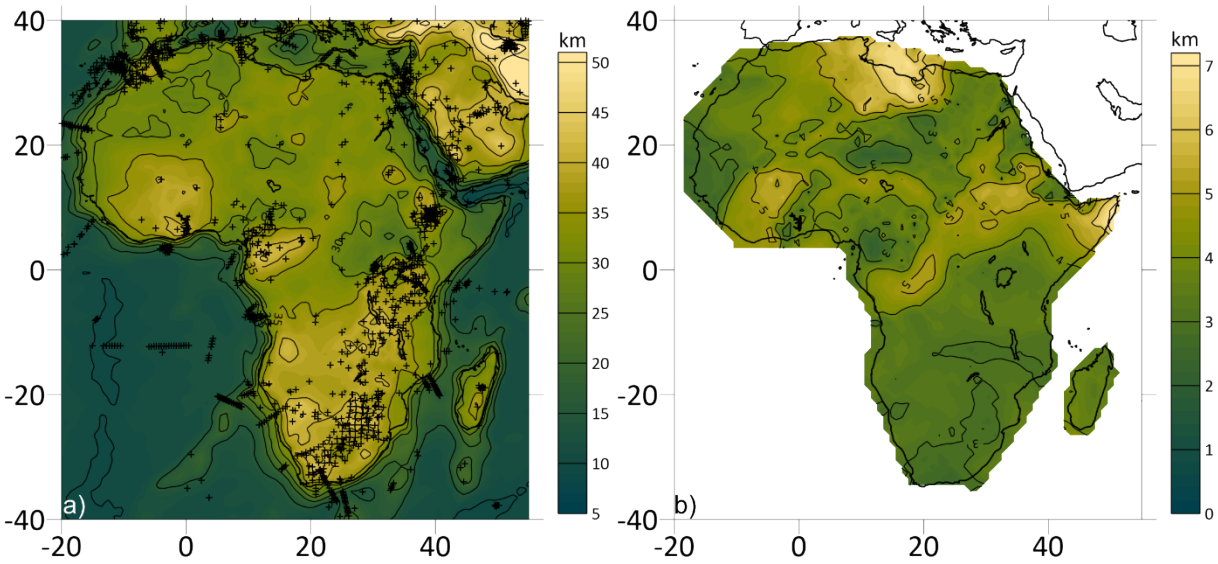

Figure 3: a) Location of seismic measurements and interpolated depth to the Moho. Southern West African craton, northern Congo craton and most of central to southern Africa show depths to the Moho above 35 km. In opposite to expectations, rather thin crust is indicated by depth to Moho around 30 km in northern West African craton and central Congo craton. b) Interpolation uncertainty of the continental area. As expected, highest values occur in areas of scarce data, like northern West African craton or Horn of Africa, and in the EARS region, where measurements are heterogeneous.

1. Mantle Residuals

Residual mantle gravity and residual topography (assuming a reference density of 2.67 g/cm^3), corrected for deep mantle variations, are shown in Figure 4. As expected, the two fields appear anticorrelated. West African and Congo cratons are dominated by negative gravity residuals partially <-100 mGal with some positive values mostly less than 100 mGal in southern West African craton and northern and eastern Congo craton. Residual topography is lower than 2 km in the central regions and mostly below 3 km towards the respective eastern and western cratonic borders. The same range of values is observed for the Uganda and Tanzania cratons. Meanwhile, southern Zimbabwe craton to northern Kaapvaal craton show positive gravity residuals up to some 200 mGal in northwestern Kaapvaal craton. These are accompanied by residual topography ranging from <2 km to even negative values where highest gravity residuals are observed. In contrast, negative gravity residuals down to -150 mGal and residual topography up to some 3 km are found at southern Kaapvaal craton, while values at northern Zimbabwe craton are in the same range as in the other cratons. At the Horn of Africa, large negative gravity residuals as low as -340 mGal and high residual topography exceeding 5 km confirm that the

interpolated values for depth to the Moho in this region are too low.

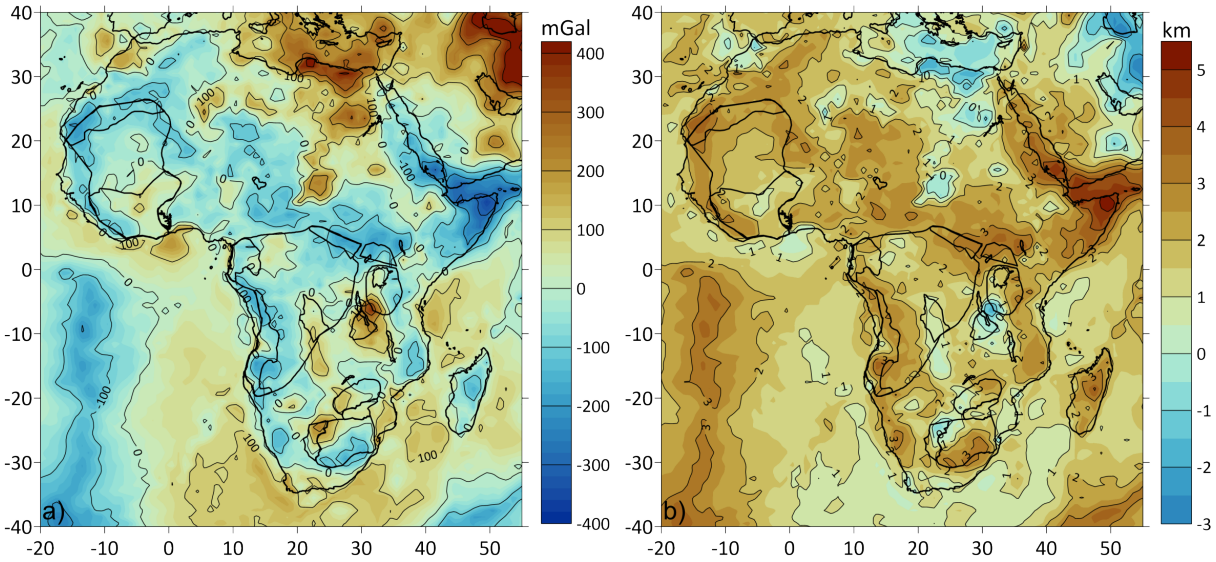

Figure 4: Residual mantle gravity (a) and residual topography (b). Extreme values at the Horn of Afrika are the result of too thin interpolated depth to Moho due to a lack of data in the region.

1. Mantle

Final results for temperature, thermal and compositional density variations as well as Mg# are presented in Figure 5. Although the modeling approach yields results from the Moho to a depth of 325 km, presentation is limited to the three layers centered at 100, 150, and 200 km depth. Results at shallow depths are strongly affected by possible uncertainties depth to Moho, while no significant compositional variations are expected at larger depths (Begg et al., 2009; Tesauro et al., 2014a). Thus, temperatures and density variations at 50, 250, and 300 km are omitted here. Density variations at 50 km are assessed later for possible adaptation of depth to the Moho. Results at great depths are included in the published data (Finger, Kaban, Tesauro, Mooney, et al., 2021).

At 100 km depth in the area of interest, temperatures below 1000 °C are present in most cratonic areas except Uganda craton and parts of Tanzania craton close to the EARS. Lowest values are found in the West African (<600 °C) and northern to central Congo cratons (<700 °C). Here, temperatures are less than 1100 °C to a depth of 200 km. In respect, strong thermal density variations up to more than 0.05 g/cm³ occur in these areas. Low temperatures occur as well at 100 km depth beneath the southern cratons with a minimum of about 800 °C in the Zimbabwe craton. They rise with increasing depth, yielding a minimum of about 1100 °C at 200 km depth and beyond 1300 °C at the southern Kaapvaal craton. Thus, existing positive thermal density variations

are less high (up to 0.04 g/cm³), and accompanied by some negative values in the high temperature areas at 200 km depth. The Saharan area not included in the West African craton, the EARS, southern Congo craton, and western coast south of it are marked by high temperatures through depths, partially exceeding 1300 °C at 100 km. At 150 km and below, temperatures above 1300 °C of the EARS extend under the Uganda and Tanzania cratons. In consequence, thermal density variations are negative in most of those areas at depths below 150 km.

High positive thermal density variations from low temperatures are compensated by negative compositional density variations and thus an increase in Mg#. These patterns are predominant in the West African, central to northern Congo, and Zimbabwe cratons at all depths. In the first, said pattern extends further northeast than one would expect based on the surface geology. In contrast, the eastern and southern Congo, Uganda, and Tanzania cratons are dominated by positive compositional variations, and no increase in Mg#. At Kaapvaal craton, negative compositional variations and increased Mg# exist at 100 km depth but retreat at larger depths, being mostly absent at 200 km.

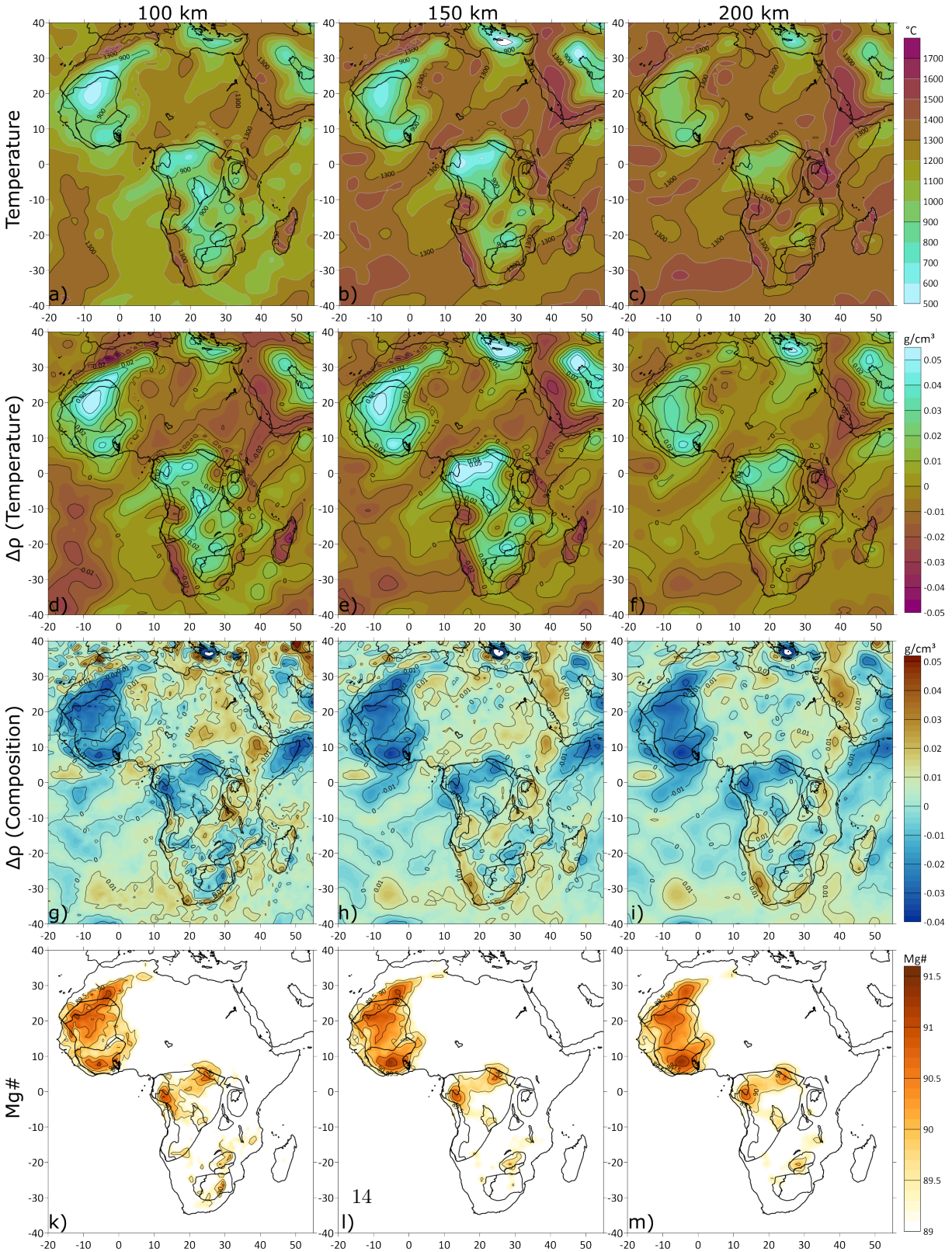
100 km
150 km
200 km
Temperature
Δρ (Temperature)
Δρ (Composition)
Mg#
°C
g/cm³
a)
b)
c)
d)
e)
f)
g)
h)
i)
k)
l)
m)

Figure 5: Final results from the iterative approach for temperature (a-c), thermal (d-f) and compositional (g-i) density variations, and Mg# (k-m) at depths of 100, 150, and 200 km (columns from left to right). Deep depleted roots are found under the West African, northern and central eastern Congo, and Zimbabwe cratons. They are absent or have been reworked at southern and easternmost Congo, Kaapvaal, Tanzania, and Uganda cratons. There is no evidence that the Bangweulu Block ever developed such a cratonic root. To ease comparison, the same colorbars are used for figures 7 and 9.

1. Improvement of the Average Crustal Density

As mentioned above, the topmost layer of the joint inversion is centered at 15 km depth and thus reveals density variations not included in the initially assumed average density of the crystalline crust taken from LITHO1.0 (Pasyanos et al., 2014). Therefore, their sum yields an improved average crustal density (Figure 6). The initial field (Figure 6a) is very heterogeneous with strong gradients, e.g., between the Tanzania craton and Bangweulu block and at northwestern Kaapvaal craton. Furthermore, several regions in the Saharan domain and the two regions just mentioned exhibit unlikely low average crustal densities less than 2.7 g/cm³. In contrast, initial average density of the crust in most cratonic areas is around 2.9 g/cm³, reaching 2.97 g/cm³. Values less than 2.85 g/cm³ are seldom observed. The inverted density variations (Figure 6b) suggest density decreases up to 0.05 g/cm³ for most cratonic areas. Density increases are suggested for cratonic areas with densities around or below 2.85 g/cm³ in the initial model. The modeling results further indicate density increases for low density parts of the Saharan domain and EARS, especially where initial densities are notably low. Therefore, the improved density model (Figure 6c) is smoother. The cratonic regions are now dominated by densities of 2.85 to 2.92 g/cm³, with some local minima down to 2.83 g/cm³. Anomalously low crustal densities in other areas of the initial model were increased to densities at least >2.75 g/cm³. Some high densities >2.9 g/cm³ of the initial model are confirmed for the central and northern Sahara, north of the Bomu-Kibali shield, Madagascar, and the eastern coast of Africa.

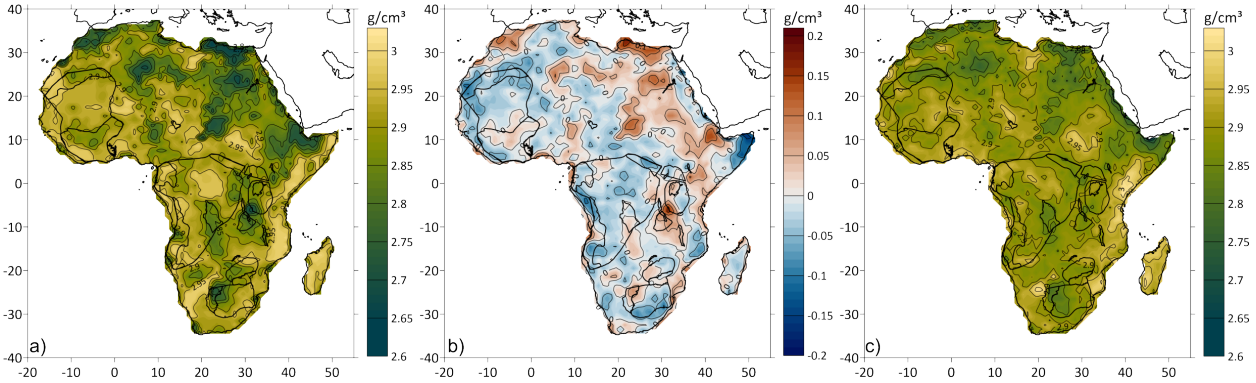

Figure 6: Improvement of average crustal density. a) Initial average crustal density from LITHO1.0 (Pasyanos et al., 2014). b) Density variations for the crust from the joint inversion. c) Sum of a) and b), giving an improved average crustal density. a) and c) use the same color scale. In general, adding the density variations leads to a smoother, less heterogeneous crystalline crust density model.

1. Main sources of Uncertainties and their Effects on Modeling Results

As mentioned in the previous chapters, the modeling approach requires certain assumptions that have some uncertainties. In the following, some main sources of such uncertainties and their effects on modeling results are discussed.

1. Depth to the Moho

The uncertainty of depth to the Moho can have a significant effect on the inversion results. For example, adding the uncertainty to the interpolated Moho depth results in thicker crust which corresponds to less total mass than in the reference model. This causes a smaller crustal gravity correction and higher mantle residuals, respectively. Also, residual topography decreases. At the same time, changing the Moho depth only has a minor effect on the thermal model, since temperatures only change if the assumed composition is changed during iterations. As a reference, Finger et al. (2021) only observed differences up to 60 K between their initial and final models. Therefore, an increase in depth to the Moho almost directly translates into higher compositional density variations and lower Mg# in the uppermost mantle, usually balanced by the opposite at greater depths. The described effects are reversed if the crust is thinned, i.e., lower compositional variations and thus higher Mg# are expected in the uppermost mantle.

Unfortunately, uncertainties of depth to Moho determinations are not always available. Comparisons in previous works (e.g., Globig et al., 2016; Jessell et al., 2016) show that most Moho depth models differ by less than 10% in areas well-covered by seismic measurements, but differences as high as 25% can occur in data devoid areas. It has to be considered that these are maximum differences between models which stem from the use of different methods and data. Thus, possible uncertainties of the depth to Moho model presented here should be considerably smaller. We use the interpolation uncertainty (Figure 3b) as a basis to assess the effects of depth to Moho uncertainties on the mantle model. In two test cases, the interpolation uncertainty is added to (M_{down}, right column in Figure 7) and subtracted from (M_{up}, left column in Figure 7) interpolated depth to the Moho (M_{base}). Residual topography and residual mantle gravity are corrected accordingly before the iterative scheme is applied. As expected, the resulting temperature fields at 100 km depth are almost indistinguishable (Figure 7a-c). Minor differences can be spotted in the southern West African and northern Congo cratons by slight changes in the shape of the 700 °C isoline. The subtle changes to the mantle model by shifting the Moho are better visible in the compositional density variations (Figure 7d-f), for example by a

larger extent of negative values (blue colors) with thinner crust. Yet, absolute differences to the final model are less than 0.01 g/cm³ for both test cases, respectively. Thus, none of the model's results are contradicted, rather confirmed. The extent of depletion with Mg# > 89.5 in the West African craton is larger than proposed based on surface geology, especially in its Northeast. Moreover, the two separate areas with Mg# > 90.5 are present in its North and South in both cases. Likewise, the Congo craton shows two areas of Mg# > 90 in the Northwest and Northeast, which appear to be not connected by Mg# > 89.5 for M_{down}. All other occurrences of increased Mg# are confirmed with slightly larger extents and values for M_{up} and respectively smaller extents and values for M_{down}.

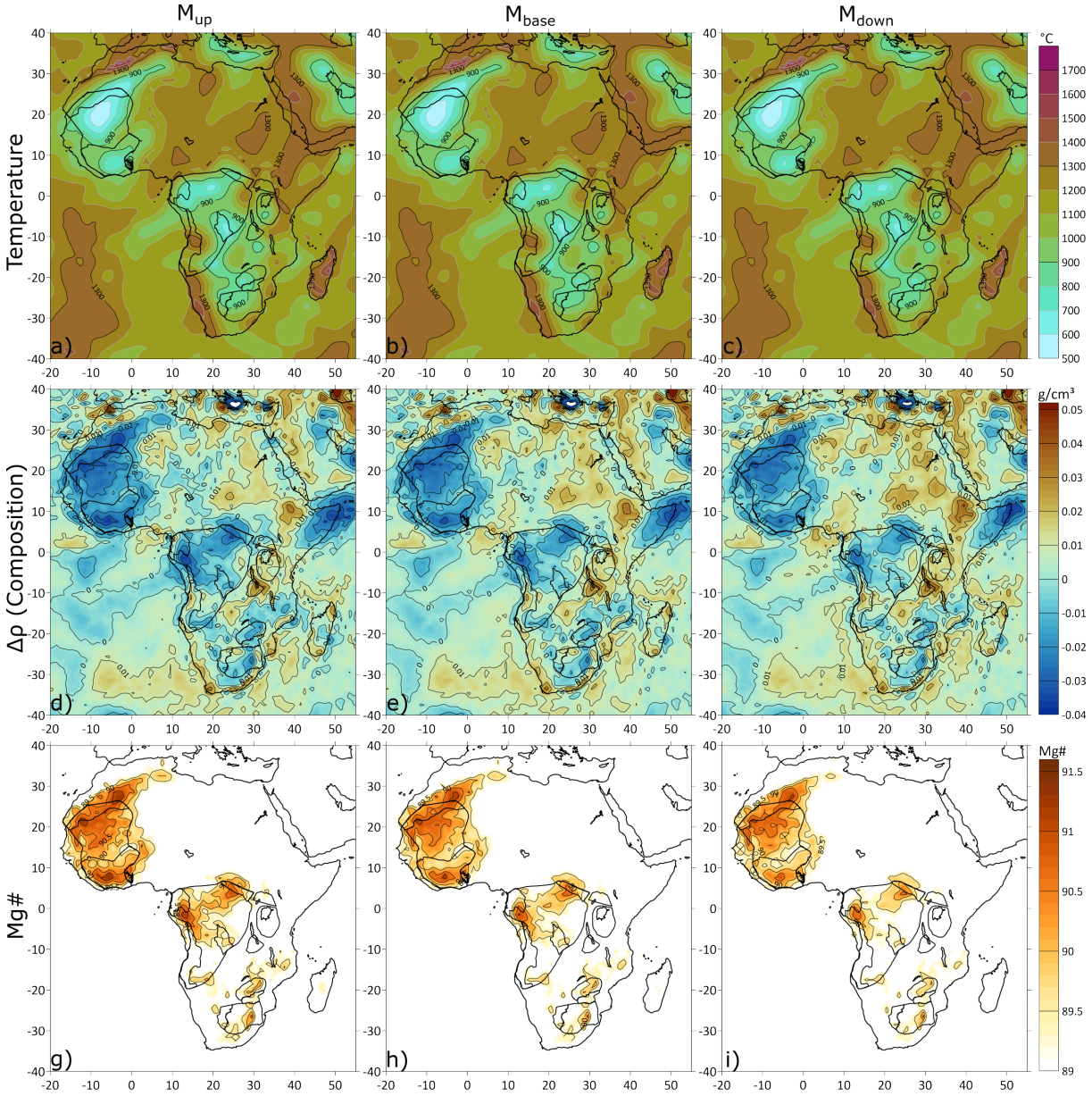

Figure 7: Temperatures (a-c), compositional variations (d-f) and Mg# (g-i) at 100 km depth for three scenarios of depth to Moho. Left and right column show results for depth to Moho shifted upwards (M_{up}) and downwards (M_{down}), respectively, by subtraction/addition of interpolation uncertainties (Figure 3b). Model results from Figure 5 (left column) are given in the middle column for comparison. Note increased extent and amplitude of negative compositional variations and Mg# for M_{up}, and a corresponding decrease for M_{down}. Colorbars

are the same as in figures 5 and 9.

Due to the absence of Moho determinations in wide parts of West African and Congo cratons, it can be assumed that a significant portion of the uppermost mantle density variations (the layer centered at 50 km) is actually caused by unmapped undulations of the Moho discontinuity. Thus, simply multiplying the compositional density variations with the quotient of layer thickness (50 km) and difference of average crustal and subcrustal densities (i.e., -0.47 g/cm^3) gives an estimate how the Moho depth would need to be modified to accommodate those density variations (Figure 8). It has to be noted, however, that this assumption is only valid in areas not sufficiently covered by seismic measurements. Otherwise, effects of Moho undulations should be minor compared to actual density variations. Therefore, points with less than two measurements within a radius of two degrees are blanked. For wide parts of West African and Congo cratons, increases (red colors) of depth to the Moho up to some 3.5 km are indicated. Values vary between -1 and 1 km in the southern West African craton. Some negative values also occur at the southwestern and eastern rims of Congo craton. This strongly indicates that interpolated depth to the Moho is too shallow for most of the two cratons. It has to be considered that proposed increments of depth to the Moho are related to negative density variations, which are generally expected in cratonic areas. Thus, the proposed increments of up to 3.5 km may provide an overestimate. Since they are mostly smaller than the interpolation uncertainty (Figure 3b), the scenarios M_{down} and M_{up} give a realistic range of possible uncertainties related to the Moho depth interpolation. Due to the increase of depth to the Moho in most of the West African and Congo cratons, M_{down} constitutes a more likely scenario than M_{up} for these cratons.

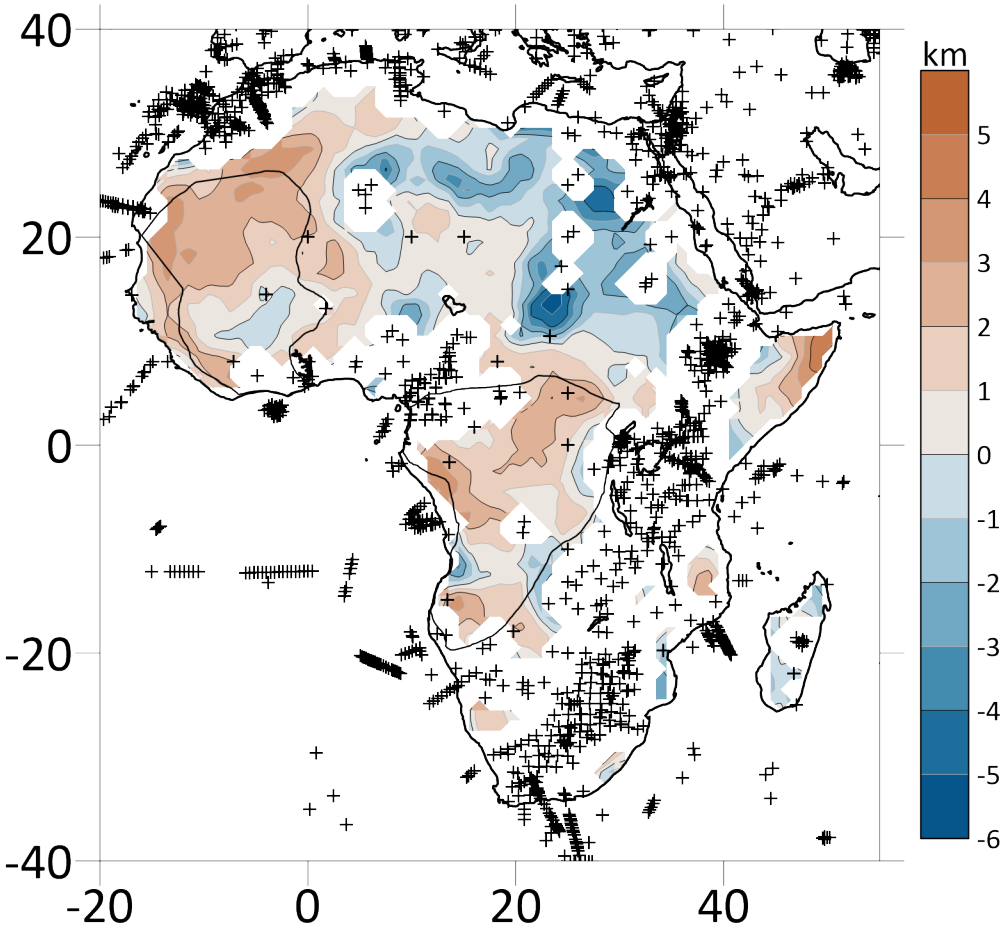

Figure 8: Indicated change of depth to the Moho, if all non-thermal density variations in the uppermost mantle were attributed to incorrect placement of the Moho discontinuity. Areas outside continental Africa and in vicinity of sufficient amount of stations (see text) are blanked. As indicated by the red colors, interpolated depth to the Moho is probably too low in wide parts of the Congo and West African cratons. High values at the Horn of Africa confirm that interpolated depth to Moho is too shallow in the area.

1. Tomography and its Conversion to Temperature

The mineral physics approach used for conversion of S-wave velocities to temperatures are influenced by various uncertainties, as described in previous studies (Finger, Kaban, Tesauro, Haeger, et al., 2021; Haeger et al., 2019; Tesauro et al., 2014a). First, the exact mantle composition is unknown since in-situ measurements are impossible. The use of an incorrect composition can induce errors up to 200 °C in highly depleted cratonic areas (Lee, 2003). In this study, un-

certainties should be around 100 °C, since only medium depletion is observed. Furthermore, the iteratively adjusted compositional model allows to mitigate this effect. In regions of temperatures above 900 °C, attenuation can cause errors around 100 °C (Jackson et al., 2002). Therefore, the attenuation models Q3 and Q4 from Cammarano et al. (2003) are applied to the "dry" cratonic (white polygon in Figure 1) and "wet", rather hot and juvenile (northern Africa except West African craton, and EARS) parts of Africa, respectively. In addition, uncertainties of about 70 °C are related to the elastic parameters and their temperature derivatives (Tesauro et al., 2014a). Finally, the underlying S-wave tomography bears its own uncertainties that could cause substantial changes to the resulting temperature model. For example, 50 m/s velocity change, which is, depending on depth, about 1.1 % of the reference S-wave velocity, can cause temperature changes of about 100 °C (Finger, Kaban, Tesauro, Haeger, et al., 2021). Unfortunately, most tomographic studies do not provide uncertainties for their results. Instead, authors commonly use spike-tests, checkerboard-tests, or synthetic models to test the resolution capacities of their models. Deviation from reference Vs seldomly exceeds -8 to +8 % in the tomography used here (Celli et al., 2020). Thus, a variation of 50 m/s already constitutes close to 7 % of the observed velocity range. Consequently, uncertainties induced by the tomographic model should be smaller than 200 °C as long as its own uncertainty remains below 14 % of the observed Vs range. In summary, assuming that some of the named error sources are mitigated by the model parametrization as described above, or may counteract each other, resulting temperature uncertainties should generally be less than 200 °C.

1. Discussion

The models presented here only reflect the current state of the mantle lithosphere. They do not allow to directly determine how or when cratonic roots have been modified, refertilized, destroyed, or if thick lithosphere previously existed. Luckily, diamondiferous kimberlites can work as proxies for the state of the lithosphere at specific times. Conveniently, sub-cratonic mantle provides the necessary temperature and pressure conditions as well as sufficiently thick lithosphere for the formation of diamondiferous kimbertites. Such kimberlites are discovered and have been analyzed on most African cratons (Begg et al., 2009; Tappe et al., 2018; De Wit et al., 2016).

1. West African Craton

Our model indicates temperatures below 1300 °C to a depth of 200 km beneath the geologically-defined West African craton. Moreover, results showing considerable depletion and temperatures less than 1100 °C indicate a larger and different subsurface extent of the West African craton than predicted based on surface geology (Figure 9 AA' and BB'; Begg et al., 2009; Ennih & Liégeois, 2008). They also confirm hypothesized lithospheric thickness considerably higher than 200 km (Steinberger & Becker, 2018). The inference of a larger extent is further confirmed by the wide area of negative compositional density variations and respectively increased Mg#. These values indicate that depleted

cratonic lithosphere is present north of the Reguibat shield (Begg et al., 2009), but does not reach the Anti Atlas, the northern limit of the West African craton proposed by Ennih & Liégeois (2008). To the Northeast, results confirm that depleted cratonic lithosphere extends up to the Mediterranean Sea (Figure 9 BB'; Celli et al., 2020). Thus, the northern limit of cratonic lithosphere parallels the Atlas Mountains, significantly exceeding the areal extent previously proposed from surface observations (Begg et al., 2009; Ennih & Liégeois, 2008). Despite temperatures still below 1300 °C at a depth of 200 km, depletion is negligible below 100 km depth in the most northeastern part. Thus, this part of the cratonic root was widely metasomatized. At its eastern boundary, negative compositional anomalies and increased Mg# terminate against the Tuareg and Nigeria Blocks, in agreement with the results of Jessell et al. (2016). In the West and South, low temperatures, negative compositional anomalies and increased Mg# are observed up to the Atlantic coast, supporting the hypothesis of a previously larger extent of the West African craton in these directions than at present (Jessell et al., 2016).

At the westernmost parts of the shields, our results differ from those of Celli et al. (2020), who argue for an absence of cratonic roots. Yet, this is no direct contradiction since their assessment is solely based on seismic velocities, whose variations are mostly caused by temperatures and the presence of melts or fluids (Goes et al., 2000). In fact, the amplitude of observed values, especially compositional variations and Mg#, decreases towards the coast. Thus, we argue that the cratonic lithosphere was in parts reworked, metasomatized and probably thinned, but is still about 200 km thick and depleted.

Finally, previous work did not find evidence for a connection of the northern Reguibat and southern Man-Leo shields at depth (Celli et al., 2020; Jessell et al., 2016). Two distinct local temperature minima under them with slightly higher temperatures in between indicate two separate roots for the West African craton (Figure 9 AA'). This pattern occurs as well in the density variations (thermal and compositional) and Mg# down to 150 km depth. At 200 km, a distinction of two bodies may only be made by means of Mg#. Thus, we conclude that the present-day West African craton originates from the amalgamation of two cratonic bodies, whose separate root structures are preserved.

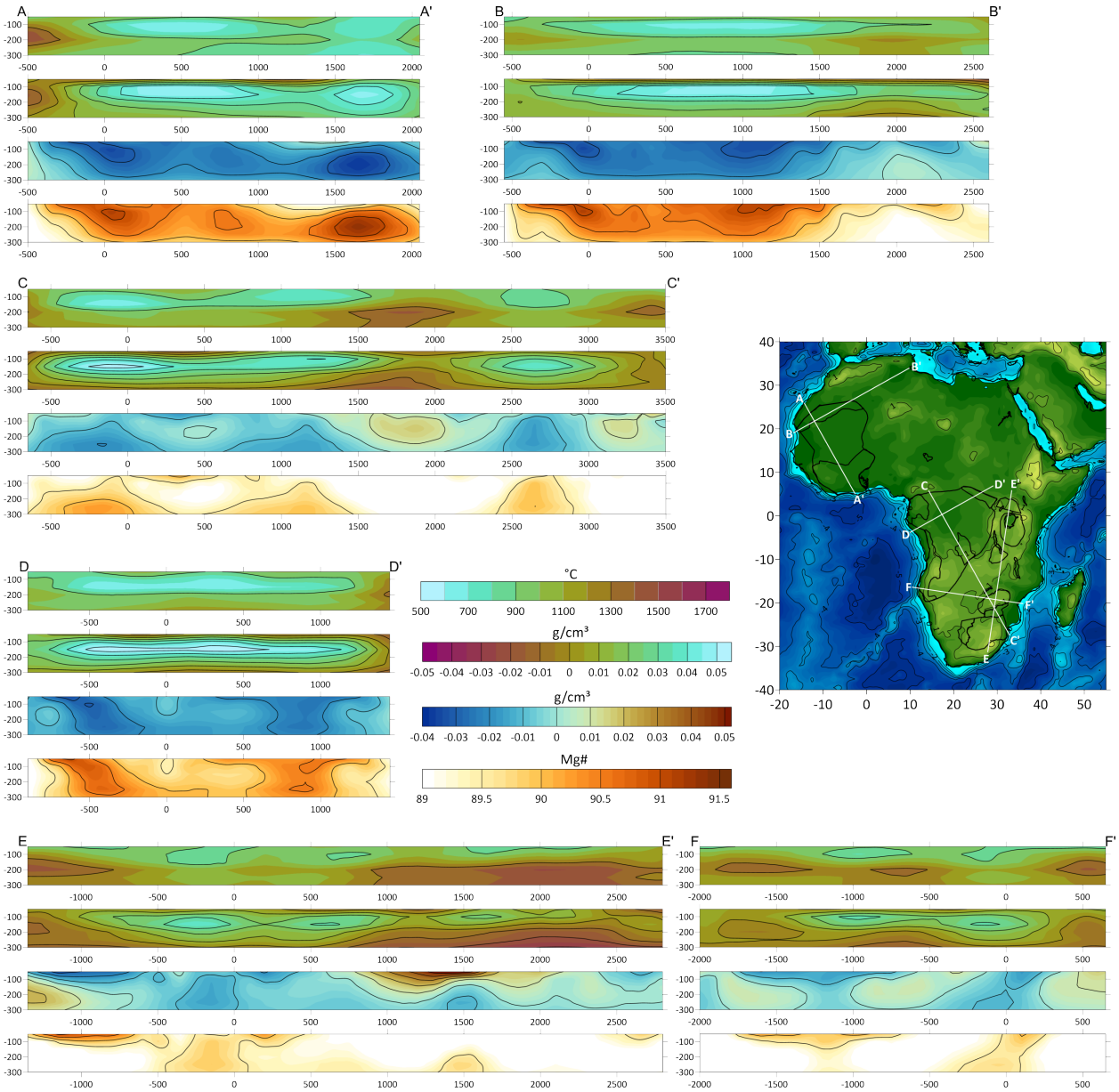

Figure 9: 2D profiles through the final mantle models of temperature, thermal density variations, compositional density variations, and Mg# (top to bottom, respectively). For location see inset topography map. Along the horizontal axis, profile km 0 marks point of orthogonal intersection of profiles AA' and BB', CC' and DD', as well as EE' and FF'. Colorbars are the same as in figures 5 and 7.

1. Congo Craton

Temperatures less than 1300 °C down to 200 km in the North and towards the central East of the Congo craton confirm the presence of thick lithosphere (Celli et al., 2020). In the East, towards the Tanzania craton, temperatures are up to 400 °C higher than at or close to the northwestern Gabon-Cameroon, northeastern Bomu-Kibali and central eastern Kasai shields and exceed 1300 °C at 200 km depth. This indicates heating from the East, probably related to the southern end of the EARS. Four local minima of compositional variations and increased Mg# of which those under or at the Gabon-Cameroon, Bomu-Kibali, and Kasai shields persist through depths, confirm the origin of the Congo craton by the amalgamation of separate cratonic terranes (Begg et al., 2009 and references therein). Further, compositional variations and Mg# indicate that the lithosphere of the Gabon-Cameroon and Bomu-Kibali shields was merged into a single block of cold lithosphere during Congo craton formation, but previous root structures were preserved, comparable to the West African craton (Figure 9 AA' and DD'). Modest negative compositional variations also lead to slightly increased Mg# between the Gabon-Cameroon and Kasai shields (Figure 9 CC'), but are absent between the latter and the Bomu-Kibali shield. Thus, we argue that during formation of the Congo craton both the Kasai and Bomu-Kibali shields and their roots accreated to the northwestern Gabon-Cameroon shield followed by cooling and thickening of the lithosphere between them. Later, rifting between the Bomu-Kibali and Kasai shields caused the formation of the Congo basin (Delvaux et al., 2021). Subsequent asthenospheric upwelling could have contributed to metasomatization of their lithospheric roots (Maddaloni et al., 2021) and thus extended the area between them where depletion is absent. However, depletion of the roots of the Congo craton shields must have taken place before craton formation. The obtained results also indicate different extents and evolution of the cratonic lithosphere of the Archean shields of the Congo Craton. For the Gabon-Cameroon shield, minimal temperatures are located at its southeastern end, strongly increasing to the Northwest, where they reach up to 1300 °C at all depths. In addition, depletion is absent in its northwestern half, although previous presence of thick cratonic lithosphere can be inferred from 2.8 Ga old kimberlites (Tappe et al., 2018). Since its formation, the northern part of the Gabon-Cameroon shield has been subjected to several tectonic processes, possibly including subduction of its northernmost part and subsequent slab detachment (Goussi Ngalamo et al., 2017) that could explain the absence of depletion. Areas of depletion and negative compositional density variations denote a large ovoid NNW-SSE cratonic root under the Gabon-Cameroon shield, stretching along the northern Angola shield, encompassing only its northern tip. Thus, it appears that a depleted cratonic root was already absent under the northern Angola shield at Congo craton formation. Furthermore, the part of the Congo craton related to the Gabun-Cameroon shield is significantly larger than one would expect from its exposed surface. Variations related to the Bomu-Kibali shield also imply an ovoid depleted root, stretching from beyond its northeastern boundary to the central northern Congo craton. Interestingly, the temperature minimum located closest to the area of strongest depletion of the root is found several hundred km to the West. Minor negative

compositional density variations in the East and the abovementioned heating from the EARS indicate reworking of the easternmost Bomu-Kibali lithosphere. To the South, mantle under the Kasai shield appears to be mostly reworked based on up to 200° higher temperatures, along with less negative compositional density variations and thus lower Mg# that are mostly confined to the shield's surface extent. Below the central Angolan shield, temperatures above 1300 °C are found at 100 km depth and dominate the southern Congo craton at a depth of 200 km from the Kasai shield to the Atlantic. Here, depletion is limited to a small area at 100 km depth of southernmost Congo craton (Figure 9 FF'). This is probably a remnant of a depleted cratonic root that was completely removed by the Tristan da Cunha plume (Celli et al., 2020), which is the likely cause of the 135 Ma Paranà-Etendeka flood basalts (Morgan, 1983). Removal of the cratonic root at an earlier time is unlikely, since thick lithosphere was required up to this time based on kimberlite ages of 124 to 135 Ma (Celli et al., 2020; Tappe et al., 2018). The Etendeka flood basalts located in this area are the counterpart to the South American Parana flood basalts. Thick and depleted lithosphere was found at the Paranapanema craton (Finger, Kaban, Tesauro, Haeger, et al., 2021), where abundant basalts have been erupted. This demonstrates that the eruption and emplacement of large quantities of basaltic magma are not sufficient per se to fully remove a cratonic root. Yet, a strong and long-lasting heat source is able to partially melt such a cratonic root and recycle it into the convecting mantle.

1. Kaapvaal and Zimbabwe cratons

Although the isopycnic hypothesis might not be valid for the Kaapvaal craton (Schutt & Lesher, 2010), our obtained results fit well to previous findings. It is evident from several studies (e.g., Brey & Shu, 2018; Griffin, O'Reilly, Natapov, et al., 2003; Lazarov et al., 2009; Weiss et al., 2021) that the present-day Kaapvaal craton is the result of several depletion episodes followed by a range of metasomatic refertilizations. Thus, values of Mg# up to 90.5 at 100 km depth probably mark remnants of the depleted cratonic root (Figure 9 EE'). Since kimberlite compositions confirm the presence of a thick depleted lithosphere up to about 80 Ma (Griffin, O'Reilly, Natapov, et al., 2003), its widespread refertilization must have occurred afterwards (Celli et al., 2020). Lithospheric thickness is still debated (e.g., Sodoudi et al., 2013; White-Gaynor et al., 2021), with estimates ranging from up to 300 km (James et al., 2001) to 170 km (Priestley et al., 2008). Concordant with the latter estimate, temperatures close to or above 1300 °C deeper than 150 km beneath most parts of the Kaapvaal craton indicate lithosphere thicknesses between 150 and 200 km. At the Zimbabwe craton, depleted cratonic lithosphere appears thick and intact, with temperatures less than 1300 °C down to 200 km of depth and Mg# up to 90. However, the imaged area of depletion appears smaller than the cratons surface extent, indicating that the Zimbabwe craton also underwent reworking.

1. Uganda and Tanzania craton

Temperatures exceed 1300 °C at a depth of 150 km beneath the Uganda and

Tanzania cratons. Along with an absence of depletion at all depths this points to complete loss of any previously existing root and a thinned lithosphere (Figure 9 EE'). Yet, temperatures below 1000 °C at 100 km depth imply that at least the Tanzania craton was underlain by thick depleted lithosphere until about 30 Ma, close to the time of plume impingement (Rooney, 2017), as confirmed by the age and composition of kimberlites (Gibson et al., 2013; Tappe et al., 2018). The existence of strong cratonic lithosphere at this time would also provide an explanation for the new plate boundary running between the Congo and Tanzania cratons instead of breaking apart the cratonic root of the Tanzania craton. Ongoing lithosphere erosion may be present due to the nearby mantle plume that is responsible for the existence of the EARS. This isindicated by the west-east increasing gradients of temperature and lithospheric thickness estimated in other studies (Boyce et al., 2021; Celli et al., 2020). The Archean Bangweulu microcontinent located southwest of the Tanzania craton appears to exhibit somewhat thicker lithosphere than Uganda and Tanzania cratons as evidenced by temperatures less than 1300 °C to a depth of 150 km. Yet, neither estimates of lithospheric depletion nor kimberlites provide evidence that a cratonic root ever existed. If it did, it was eroded completely without presently detectable remnants. Such erosion appears possible in view of the fact that the microcontinent was heavily deformed by the surrounding Proterozoic belts (Begg et al., 2009).

1. Conclusions

In this work, recent S-wave tomography was combined with satellite gravity and crustal data to obtain self-consistent models of temperatures, thermal and compositional density variations, and Mg# for the African upper mantle down to 325 km, focusing on its cratonic parts. In addition, a new, purely seismic model of depth to the Moho was calculated and an improved model of average crustal densities obtained. Depth to the Moho is in the range of 35-42 km in most cratonic regions, except the central to northeastern Congo and northern West African cratons. For these regions, mantle modeling results indicated that depths to the Moho, in parts as low as 28 km, are underestimated due to a lack of sufficient seismic measurements. Average crystalline crust densities of the cratonic areas are 2.85 to 2.92 g/cm^3 in most cratonic areas. Lower values (around 2.83 g/cm^3) occur at the Reguibat (northern West African craton) and Kasai (eastern Congo craton) shields as well as western Kaapvaal craton. An assessment of the effects of uncertainties in the depth to Moho and the velocity-temperature conversion showed that they do not qualitatively affect the primary results presented here concerning the physical state of the African cratonic roots.

Deep depleted lithospheric roots were found under the Reguibat and Man-Leo shields of the West African craton, the Gabon-Cameroon, Bomu-Kibali, and Kasai shields of the Congo craton, and Zimbabwe craton. In these regions, temperatures range from less than 700 °C at 100 km depth to less than 1200 °C at 200 km depth, accompanied by compositional variations between -0.01 and -0.035 g/cm^3, which indicate values of Mg# from 89.5 to 91.4, respectively.

The identification of separate cratonic roots under the Archean shields of the Congo and West African cratons provides strong evidence that depletion of these roots occurred before they were amalgamated into the larger cratons. Some depletion was imaged at the southernmost Angolan shield of the Congo craton and at Kaapvaal craton, but vanishes with temperatures exceeding 1300 °C at or below 150 km of depth, and is absent beneath the Uganda and Tanzania cratons. Previously existing cratonic roots in these areas were largely reworked or completely removed, the most likely cause being mantle plumes, as evidenced by active volcanism or flood basalts.

Acknowledgments

We thank Nicolas Celli for sharing shapefiles of the African cratonic areas. This work was financed by the German Research Foundation (DFG), grant KA 2669/6-1 (project number 336717379). This study employs color vision deficiency friendly colorbars (Crameri et al., 2020) to improve accessibility and reduce risk of misinterpretation.

Open Research

Upon acceptance, data associated with this article will be made available via GFZ Data Services (Finger, Kaban, Tesauro, Mooney, et al., 2021): https://doi.org/https://doi.org/10.5880/GFZ.1.3.2021.006.

References

Amante, C., & Eakins, B. W. (2009). ETOPO1 1 Arc-Minute Global Relief Model: Procedures, Data Sources and Analysis. *NOAA Technical Memorandum NESDIS NGDC-24*, (March), 19. https://doi.org/10.1594/PANGAEA.769615Begg, G. C., Griffin, W. L., Natapov, L. M., O'Reilly, S. Y., Grand, S. P., O'Neill, C. J., et al. (2009). The lithospheric architecture of Africa: Seismic tomography, mantle petrology, and tectonic evolution. *Geosphere*, *5*(1), 23–50. https://doi.org/10.1130/GES00179.1Boyce, A., Bastow, I. D., Cottaar, S., Kounoudis, R., Courbeville, J. G. De, Caunt, E., & Desai, S. (2021). AFRP20: New P-Wavespeed Model for the African Mantle Reveals Two Whole-Mantle Plumes Below East Africa and Neoproterozoic Modification of the Tanzania Craton. *Geochemistry, Geophysics, Geosystems*, *22*(3), e2020GC009302. https://doi.org/10.1029/2020GC009302Brey, G. P., & Shu, Q. (2018). The birth, growth and ageing of the Kaapvaal subcratonic mantle. *Mineralogy and Petrology 2018 112:1*, *112*(1), 23–41. https://doi.org/10.1007/S00710-018-0577-8Cammarano, F., Goes, S., Vacher, P., & Giardini, D. (2003). Inferring upper-mantle temperatures from seismic velocities. *Physics of the Earth and Planetary Interiors*, *138*(3–4), 197–222. https://doi.org/10.1016/S0031-9201(03)00156-0Celli, N. L., Lebedev, S., Schaeffer, A. J., & Gaina, C. (2020). African cratonic lithosphere carved by mantle

plumes. *Nature Communications*, *11*(1), 92. https://doi.org/10.1038/s41467-019-13871-2Crameri, F., Shephard, G. E., & Heron, P. J. (2020). The misuse of colour in science communication. *Nature Communications 2020 11:1*, *11*(1), 1–10. https://doi.org/10.1038/s41467-020-19160-7Delvaux, D., Maddaloni, F., Tesauro, M., & Braitenberg, C. (2021). The Congo Basin: Stratigraphy and subsurface structure defined by regional seismic reflection, refraction and well data. *Global and Planetary Change*, *198*(December 2020), 103407. https://doi.org/10.1016/j.gloplacha.2020.103407Ebinger, C. J., & Sleep, N. H. (1998). Cenozoic magmatism throughout east Africa resulting from impact of a single plume. *Nature*, *395*(6704), 788–791. https://doi.org/10.1038/27417Ennih, N., & Liégeois, J.-P. (2008). The boundaries of the West African craton, with special reference to the basement of the Moroccan metacratonic Anti-Atlas belt. *Geological Society, London, Special Publications*, *297*(1), 1–17. https://doi.org/10.1144/SP297.1Finger, N.-P., Kaban, M. K., Tesauro, M., Haeger, C., Mooney, W. D., & Thomas, M. (2020). A Thermo-Compositional Model of the Cratonic Lithosphere of South America: Models of the Upper Mantle, Crust and Sediment Density. GFZ Data Services. https://doi.org/10.5880/GFZ.1.3.2020.006Finger, N.-P., Kaban, M. K., Tesauro, M., Haeger, C., Mooney, W. D., & Thomas, M. (2021). A Thermo-Compositional Model of the Cratonic Lithosphere of South America. *Geochemistry, Geophysics, Geosystems*, *22*(4), e2020GC009307. https://doi.org/10.1029/2020GC009307Finger, N.-P., Kaban, M. K., Tesauro, M., Mooney, W. D., & Thomas, M. (2021). Thermo-Compositional Model of Cratonic Lithosphere and Depth to Moho of Africa. Potsdam: GFZ Data Services. https://doi.org/https://doi.org/10.5880/GFZ.1.3.2021.006Fishwick, S. (2010). Surface wave tomography: Imaging of the lithosphere–asthenosphere boundary beneath central and southern Africa? *Lithos*, *120*(1–2), 63–73. https://doi.org/10.1016/J.LITHOS.2010.05.011Förste, C., Bruinsma, S., Abrikosov, O., Flechtner, F., Marty, J.-C., Lemoine, J.-M., et al. (2014). *EIGEN-6C4-The latest combined global gravity field model including GOCE data up to degree and order 1949 of GFZ Potsdam and GRGS Toulouse. Geophysical Research Abstracts* (Vol. 16). Retrieved from http://icgem.gfz-potsdam.deGibson, S. A., McMahon, S. C., Day, J. A., & Dawson, J. B. (2013). Highly Refractory Lithospheric Mantle beneath the Tanzanian Craton: Evidence from Lashaine Pre-metasomatic Garnet-bearing Peridotites. *Journal of Petrology*, *54*(8), 1503–1546. https://doi.org/10.1093/PETROLOGY/EGT020Giuliani, A., Phillips, D., Maas, R., Woodhead, J. D., Kendrick, M. A., Greig, A., et al. (2014). LIMA U–Pb ages link lithospheric mantle metasomatism to Karoo magmatism beneath the Kimberley region, South Africa. *Earth and Planetary Science Letters*, *401*, 132–147. https://doi.org/10.1016/J.EPSL.2014.05.044Globig, J., Fernàndez, M., Torne, M., Vergés, J., Robert, A., & Faccenna, C. (2016). New insights into the crust and lithospheric mantle structure of Africa from elevation, geoid, and thermal analysis. *Journal of Geophysical Research: Solid Earth*, *121*(7), 5389–5424. https://doi.org/10.1002/2016JB012972Goes, S., Govers, R., & Vacher, P. (2000). Shallow mantle temperatures under Europe from P and

S wave tomography. *Journal of Geophysical Research: Solid Earth*, *105*(B5), 11153–11169. https://doi.org/10.1029/1999JB900300Goussi Ngalamo, J. F., Bisso, D., Abdelsalam, M. G., Atekwana, E. A., Katumwehe, A. B., & Ekodeck, G. E. (2017). Geophysical imaging of metacratonizaton in the northern edge of the Congo craton in Cameroon. *Journal of African Earth Sciences*, *129*, 94–107. https://doi.org/10.1016/J.JAFREARSCI.2016.12.010Griffin, W. L., O'Reilly, S. Y., Natapov, L. M., & Ryan, C. G. (2003). The evolution of lithospheric mantle beneath the Kalahari Craton and its margins. *Lithos*, *71*(2–4), 215–241. https://doi.org/10.1016/J.LITHOS.2003.07.006Griffin, W. L., O'Reilly, S. Y., Abe, N., Aulbach, S., Davies, R. M., Pearson, N. J., et al. (2003). The origin and evolution of Archean lithospheric mantle. *Precambrian Research*, *127*(1–3), 19–41. https://doi.org/10.1016/S0301-9268(03)00180-3Haeger, C., & Kaban, M. K. (2019). Decompensative Gravity Anomalies Reveal the Structure of the Upper Crust of Antarctica. *Pure and Applied Geophysics*, *176*(10), 4401–4414. https://doi.org/10.1007/s00024-019-02212-5Haeger, C., Kaban, M. K., Tesauro, M., Petrunin, A. G., & Mooney, W. D. (2019). 3-D Density, Thermal, and Compositional Model of the Antarctic Lithosphere and Implications for Its Evolution. *Geochemistry, Geophysics, Geosystems*, *20*(2), 688–707. https://doi.org/10.1029/2018GC008033Hu, J., Liu, L., Faccenda, M., Zhou, Q., Fischer, K. M., Marshak, S., & Lundstrom, C. (2018). Modification of the Western Gondwana craton by plume-lithosphere interaction. *Nature Geoscience*, *11*(3), 203–210. https://doi.org/10.1038/s41561-018-0064-1Hyndman, R. D., Currie, C. A., Mazzotti, S., & Frederiksen, A. (2009). Temperature control of continental lithosphere elastic thickness, Te vs Vs. *Earth and Planetary Science Letters*, *277*(3–4), 539–548. https://doi.org/10.1016/j.epsl.2008.11.023Jackson, I., Fitz Gerald, J. D., Faul, U. H., & Tan, B. H. (2002). Grain-size-sensitive seismic wave attenuation in polycrystalline olivine. *Journal of Geophysical Research: Solid Earth*, *107*(B12), ECV 5-1-ECV 5-16. https://doi.org/10.1029/2001jb001225James, D. E., Fouch, M. J., VanDecar, J. C., & van der Lee, S. (2001). Tectospheric structure beneath southern Africa. *Geophysical Research Letters*, *28*(13), 2485–2488. https://doi.org/10.1029/2000GL012578Jessell, M. W., Begg, G. C., & Miller, M. S. (2016). The geophysical signatures of the West African Craton. *Precambrian Research*, *274*, 3–24. https://doi.org/10.1016/J.PRECAMRES.2015.08.010Jordan, T. H. (1978). Composition and development of the continental tectosphere. *Nature*, *274*(5671), 544–548. https://doi.org/10.1038/274544a0Kaban, M. K., & Mooney, W. D. (2001). Density structure of the lithosphere in the southwestern United States and its tectonic significance. *Journal of Geophysical Research: Solid Earth*, *106*(B1), 721–739. https://doi.org/10.1029/2000JB900235Kaban, M. K., Tesauro, M., Mooney, W. D., & Cloetingh, S. A. P. L. (2014). Density, temperature, and composition of the North American lithosphere-New insights from a joint analysis of seismic, gravity, and mineral physics data: 1. Density structure of the crust and upper mantle. *Geochemistry, Geophysics, Geosystems*, *15*(12), 4781–4807. https://doi.org/10.1002/2014GC005483Kaban, M. K., Mooney, W. D., & Petrunin, A. G. (2015). Cratonic root beneath

North America shifted by basal drag from the convecting mantle. *Nature Geoscience*, *8*(10), 797–800. https://doi.org/10.1038/ngeo2525Kaban, M. K., Stolk, W., Tesauro, M., El Khrepy, S., Al-Arifi, N., Beekman, F., & Cloetingh, S. A. P. L. (2016). 3D density model of the upper mantle of Asia based on inversion of gravity and seismic tomography data. *Geochemistry, Geophysics, Geosystems*, *17*(11), 4457–4477. https://doi.org/10.1002/2016GC006458Kaban, M. K., El Khrepy, S., & Al-Arifi, N. (2016). Isostatic Model and Isostatic Gravity Anomalies of the Arabian Plate and Surroundings. *Pure and Applied Geophysics*, *173*(4), 1211–1221. https://doi.org/10.1007/s00024-015-1164-0Laske, G., Masters, G., Ma, Z., & Pasyanos, M. (2013). Update on CRUST1.0---A 1-degree global model of Earth's crust. In *EGU General Assembly 2013* (Vol. 15, p. 2658). Retrieved from https://ui.adsabs.harvard.edu/abs/2013EGUGA..15.2658L/abstractLazarov, M., Brey, G. P., & Weyer, S. (2009). Time steps of depletion and enrichment in the Kaapvaal craton as recorded by subcalcic garnets from Finsch (SA). *Earth and Planetary Science Letters*, *279*(1–2), 1–10. https://doi.org/10.1016/J.EPSL.2008.12.015Lee, C.-T. A. (2003). Compositional variation of density and seismic velocities in natural peridotites at STP conditions: Implications for seismic imaging of compositional heterogeneities in the upper mantle. *Journal of Geophysical Research: Solid Earth*, *108*(B9). https://doi.org/10.1029/2003jb002413Lee, C.-T. A., Luffi, P., & Chin, E. J. (2011). Building and Destroying Continental Mantle. *Annual Review of Earth and Planetary Sciences*, *39*(1), 59–90. https://doi.org/10.1146/annurev-earth-040610-133505Maddaloni, F., Braitenberg, C., Kaban, M. K., Tesauro, M., & Delvaux, D. (2021). The Congo Basin: Subsurface structure interpreted using potential field data and constrained by seismic data. *Global and Planetary Change*, *205*(July), 103611. https://doi.org/10.1016/j.gloplacha.2021.103611McDonough, W. F., & Sun, S. s. (1995). The composition of the Earth. *Chemical Geology*, *120*(3–4), 223–253. https://doi.org/10.1016/0009-2541(94)00140-4van der Meijde, M., Fadel, I., Ditmar, P., & Hamayun, M. (2015). Uncertainties in crustal thickness models for data sparse environments: A review for South America and Africa. *Journal of Geodynamics*, *84*, 1–18. https://doi.org/10.1016/J.JOG.2014.09.013Mooney, W. D. (2015). Crust and Lithospheric Structure - Global Crustal Structure. In G. Schubert, B. Romanowicz, & A. Dziewonski (Eds.), *Treatise on Geophysics* (2nd ed., pp. 339–390). Elsevier.Mooney, W. D., & Kaban, M. K. (2010). The North American upper mantle: Density, composition, and evolution. *Journal of Geophysical Research*, *115*(B12), B12424. https://doi.org/10.1029/2010JB000866Mooney, W. D., & Vidale, J. E. (2003). Thermal and chemical variations in subcrustal cratonic lithosphere: evidence from crustal isostasy. *Lithos*, *71*(2–4), 185–193. https://doi.org/10.1016/J.LITHOS.2003.07.004Morgan, W. J. (1983). Hotspot Tracks and the Early Rifting of the Atlantic. *Developments in Geotectonics*, *19*(C), 123–139. https://doi.org/10.1016/B978-0-444-42198-2.50015-8Murphy, B., Müller, S., & Yurchak, R. (2020). GeoStat-Framework/PyKrige: v1.5.0. https://doi.org/10.5281/ZENODO.3739879Pasyanos, M. E., & Nyblade, A. A.

(2006). A top to bottom lithospheric study of Africa and Arabia. *Undefined*, *444*(1–4), 27–44. https://doi.org/10.1016/J.TECTO.2007.07.008Pasyanos, M. E., Masters, T. G., Laske, G., & Ma, Z. (2014). LITHO1.0: An updated crust and lithospheric model of the Earth. *Journal of Geophysical Research: Solid Earth*, *119*(3), 2153–2173. https://doi.org/10.1002/2013JB010626Priestley, K., Mckenzie, D., Debayle, E., & Pilidou, S. (2008). The African upper mantle and its relationship to tectonics and surface geology. *Geophysical Journal International*, *175*(3), 1108–1126. https://doi.org/10.1111/J.1365-246X.2008.03951.XRitsema, J., Deuss, A., van Heijst, H. J., & Woodhouse, J. H. (2011). S40RTS: a degree-40 shear-velocity model for the mantle from new Rayleigh wave dispersion, teleseismic traveltime and normal-mode splitting function measurements. *Geophysical Journal International*, *184*(3), 1223–1236. https://doi.org/10.1111/j.1365-246X.2010.04884.xRooney, T. O. (2017). The Cenozoic magmatism of East-Africa: Part I — Flood basalts and pulsed magmatism. *Lithos*, *286–287*, 264–301. https://doi.org/10.1016/J.LITHOS.2017.05.014Root, B. C., Novák, P., Dirkx, D., Kaban, M. K., van der Wal, W., & Vermeersen, L. L. A. (2016). On a spectral method for forward gravity field modelling. *Journal of Geodynamics*, *97*, 22–30. https://doi.org/10.1016/J.JOG.2016.02.008Schaeffer, A. J., & Lebedev, S. (2013). Global shear speed structure of the upper mantle and transition zone. *Geophysical Journal International*, *194*(1), 417–449. https://doi.org/10.1093/gji/ggt095Schutt, D. L., & Lesher, C. E. (2010). Compositional trends among Kaapvaal Craton garnet peridotite xenoliths and their effects on seismic velocity and density. *Earth and Planetary Science Letters*, *300*(3–4), 367–373. https://doi.org/10.1016/J.EPSL.2010.10.018Sodoudi, F., Yuan, X., Kind, R., Lebedev, S., Adam, J. M. C., Kästle, E., & Tilmann, F. (2013). Seismic evidence for stratification in composition and anisotropic fabric within the thick lithosphere of Kalahari Craton. *Geochemistry, Geophysics, Geosystems*, *14*(12), 5393–5412. https://doi.org/10.1002/2013GC004955Steinberger, B., & Becker, T. W. (2018). A comparison of lithospheric thickness models. *Tectonophysics*, *746*, 325–338. https://doi.org/10.1016/j.tecto.2016.08.001Stixrude, L., & Lithgow-Bertelloni, C. (2005, August 1). Thermodynamics of mantle minerals - I. Physical properties. *Geophysical Journal International*. Narnia. https://doi.org/10.1111/j.1365-246X.2005.02642.xStolk, W., Kaban, M. K., Beekman, F., Tesauro, M., Mooney, W. D., & Cloetingh, S. (2013). High resolution regional crustal models from irregularly distributed data: Application to Asia and adjacent areas. *Tectonophysics*, *602*, 55–68. https://doi.org/10.1016/j.tecto.2013.01.022Tappe, S., Smart, K., Torsvik, T., Massuyeau, M., & de Wit, M. (2018). Geodynamics of kimberlites on a cooling Earth: Clues to plate tectonic evolution and deep volatile cycles. *Earth and Planetary Science Letters*, *484*, 1–14. https://doi.org/10.1016/j.epsl.2017.12.013Tesauro, M., Kaban, M. K., Mooney, W. D., & Cloetingh, S. A. P. L. (2014a). Density, temperature, and composition of the North American lithosphere-New insights from a joint analysis of seismic, gravity, and mineral physics data: 2. Thermal and composi-

tional model of the upper mantle. *Geochemistry, Geophysics, Geosystems*, *15*(12), 4808–4830. https://doi.org/10.1002/2014GC005484Tesauro, M., Kaban, M. K., Mooney, W. D., & Cloetingh, S. (2014b). NACr14: A 3D model for the crustal structure of the North American Continent. *Tectonophysics*, *631*, 65–86. https://doi.org/10.1016/j.tecto.2014.04.016Tesauro, M., Kaban, M. K., & Aitken, A. R. A. (2020). Thermal and Compositional Anomalies of the Australian Upper Mantle From Seismic and Gravity Data. *Geochemistry, Geophysics, Geosystems*, *21*(11), e2020GC009305. https://doi.org/10.1029/2020GC009305Tugume, F., Nyblade, A., Julià, J., & van der Meijde, M. (2013). Precambrian crustal structure in Africa and Arabia: Evidence lacking for secular variation. *Tectonophysics*, *609*, 250–266. https://doi.org/10.1016/J.TECTO.2013.04.027Weiss, Y., Kiro, Y., Class, C., Winckler, G., Harris, J. W., & Goldstein, S. L. (2021). Helium in diamonds unravels over a billion years of craton metasomatism. *Nature Communications 2021 12:1*, *12*(1), 1–11. https://doi.org/10.1038/s41467-021-22860-3White-Gaynor, A. L., Nyblade, A. A., Durrheim, R. J., Raveloson, R., Meijde, M. van der, Fadel, I., et al. (2021). Shear-Wave Velocity Structure of the Southern African Upper Mantle: Implications for Craton Structure and Plateau Uplift. *Geophysical Research Letters*, *48*(7), e2020GL091624. https://doi.org/10.1029/2020GL091624Wilson, M. (1997). Thermal evolution of the Central Atlantic passive margins: Continental break-up above a Mesozoic super-plume. *Journal of the Geological Society*, *154*(3), 491–495. https://doi.org/10.1144/gsjgs.154.3.0491De Wit, M., Bhebhe, Z., Davidson, J., Haggerty, S. E., Hundt, P., Jacob, J., et al. (2016). Overview of Diamond Resources in Africa. *Episodes*, *39*(2), 199–237. https://doi.org/10.18814/epiiugs/2016/v39i2/95776